J Fail. Anal. and Preven.
https://doi.org/10.1007/s11668-023-01591-1

CASE HISTORY—PEER-REVIEWED

Failure Analysis on Premature Fracture of Polyethylene Pipe for Floor Heating System

Mao-Kai Xu · Xiang Li · Cai-Ru Feng · Xue-Ling Li · Zhen-Guo Yang

Submitted: 20 December 2022 / Accepted: 20 December 2022

Abstract Polyethylene (PE) pipes are widely used in floor heating system due to their corrosion resistance, low cost and other advantages. This paper investigated the premature fracture of PE pipe for floor heating system in a residential building in the northern part of China for only serving less than 3 years, while the design service life was 50 years. In order to ascertain the root causes of this failure, a series of macro- and micro-scope characterization methods were conducted. The comprehensive analysis results showed that failure mechanism of the failed pipe was slow crack cracking with defects. Low molecular weight and substandard molecular weight distribution are the root causes of that premature fracture. Excessive bending, fibrous inclusions and shrinkage holes in the matrix are also important causes of the failure. Subsequently, the influence of polymer molecular weight on the mechanical properties of materials and the micro-configuration response of polymer pipes under tensile stress was analyzed in depth. It is theoretically demonstrated that polymer microstructures such as molecular weight distribution fundamentally affect the properties of polymer materials, which should be paid enough attention in the process of production and use. At last, several countermeasures are thus put forward in order to enhance safety operation and reliability of the PE pipes for floor heating system.

M.-K. Xu · Z.-G. Yang (✉)
Department of Materials Science, Fudan University, Shanghai, China
e-mail: zgyang@fudan.edu.cn

X. Li · C.-R. Feng · X.-L. Li
The Inner Mongolia Autonomous Region Institute of Product Quality Inspection, Huhhot, China

Keywords Polyethylene pipe · Floor heating system · Fracture · Failure analysis

Introduction and Background

Energy conservation and green development growth have become important issues in today's international community [1–3]. In 2021, the heating sector contributed half of total carbon emission added [4]. Therefore, it is of great practical significance to improve the energy efficiency of heating system. Compared with the air condition heating system, the temperature fluctuation and temperature gradient in the vertical direction caused by the radiant heating system are relatively less, which can reduce the temperature required to achieve thermal comfort, and in turn achieves less energy consumption and carbon emission [5–7]. Of all the radiant heating systems, floor heating system is the most efficiency, does not occupy indoor space, has the advantages of aesthetics, and so on, making it being an increasingly popular heating option [8, 9].

Four major components of the floor heating system are heat source system (wall-hung boiler or heat pump), piping system (main pipe and coil), insulation system (insulation board, reflective film, boundary insulation strip), and control system (water collector, thermostat, mixing center), as shown in Fig. 1. Those four components are responsible for generating heat, heat transfer and heat dissipation, temperature maintenance, and temperature control, respectively [5]. The piping system is buried underground, so its failure has the characteristic of concealment. The commonly used piping systems for floor heating systems are aluminum-plastic pipes and PE-RT pipes. Compared with PE-RT pipes, aluminum-plastic pipes have

Published online: 09 January 2023

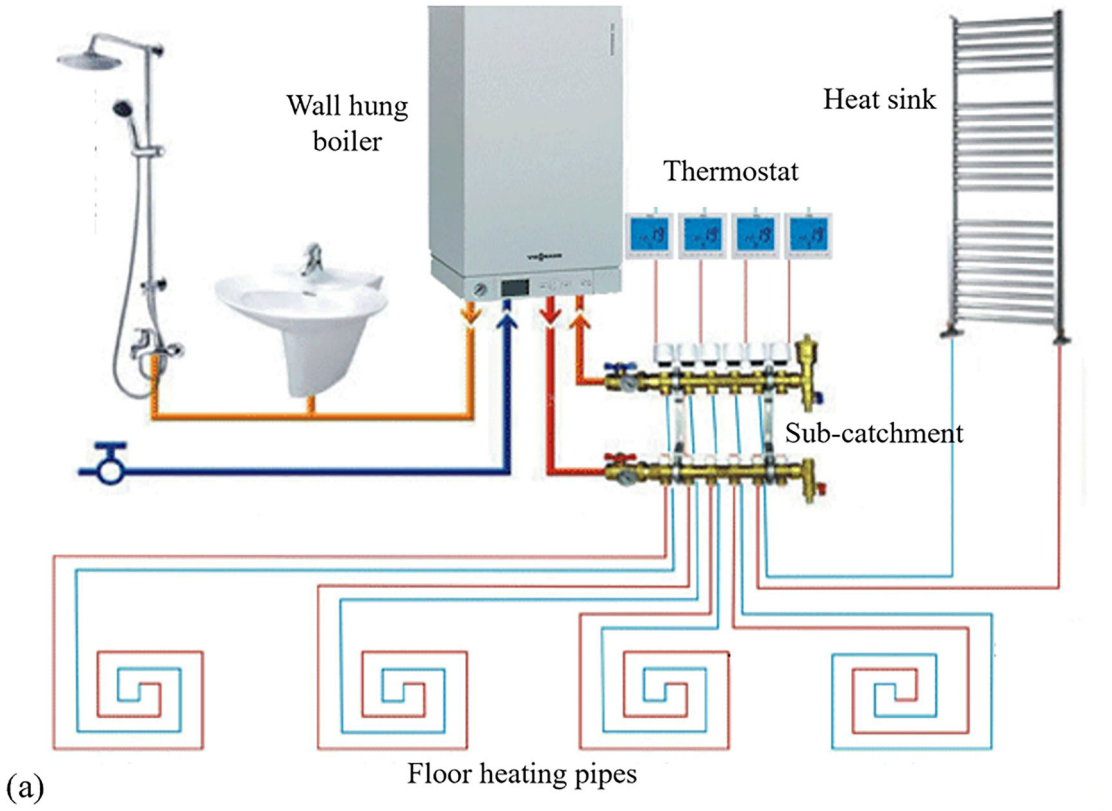

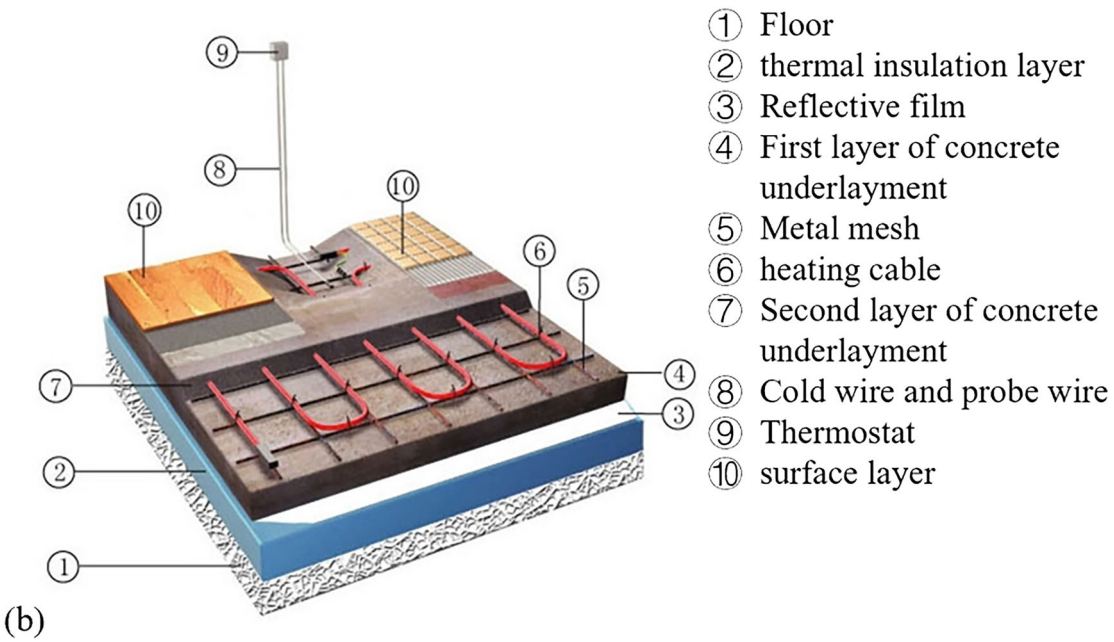

Fig. 1 Schematic diagram of floor heating system (**a**) whole, and (**b**) buried part

shortcomings such as higher cost, poorer thermal conductivity, and less stable due to the multilayer composite structure [10]. In various applications, it is safe and reliable and has been widely recognized by pipeline manufacturers, design units, thermal companies, and management departments.

In previous studies, researchers have done a lot of works on failure cases of buried PE pipes caused by disasters, third-part interference, erosion corrosion, chemical oxidation degradation, biological degradation and other factors, and the failure mechanism of buried PE pipes [11–13]. Liu et al. [14] evaluated mechanical response of buried PE pipes under excavation load during pavement construction by establishing a finite element model considering the pipe-soil interaction and showed that the PE pipes would become highly plastic stress state under the excavation load. Ya et al. [15] found that compared with steel pipe, HDPE pipe was less susceptible to erosion due to the hydrocarbon sheets were able to withstand the erosion effect of the particles in the fluid flow. Li et al. [16] studied the buried PE pipes mechanical behaviors and failure mechanisms under strike-slip fault movements. Liang et al. used the finite element method to study the mechanical behavior of PE pipes underground overload, and found that the stress and deformation behavior of buried PE pipes are related to the wall thickness, buried depth, internal pressure and other factors of the pipes [17]. Yang et al. [18] revealed that the HDPE pipes buried in humid and other favorable environment for termites might be subjected to biodegrade after being attacked by termites due to their low hardness. However, few researches have been devoted to the failure of PE pipe due to the defects on the surface and inside of the pipe, and the effect of stress on PE pipes on their fracture behavior.

This paper conducts failure analysis on a premature fracture of PE pipes for floor heating system in a residential building in northern China. The designed service life was 50 years, while multiple fractures occurred in less than three years of service. As shown in Fig. 2, the failed floor heating pipeline studied in this article is a set of coiled tubes. Coils are easier to bend than straight pipes and therefore use fewer joints, thereby improving structural integrity and safety reliability. However, due to the special structural characteristics of coils, excessive bending often occurs during construction and installation.

Based on our precious experience related to failure analysis of polymer materials, especially of PE [19, 20], comprehensive and systematic analyses were carried out to find the root causes of that failure. The results show that the unreasonable molecular weight distribution caused the mechanical properties of the floor heating pipes to fail to meet the design requirements, which was the root cause of the premature fracture. The excessive bending of the fracture region and the existence of fibrous inclusions inside were the important reasons for its failure. The defect morphology also promoted the premature fracture process. In those regards, we propose that the selection of floor heating pipe materials should be strictly based on technical standards, installation process should ensure compliance, and other related countermeasures, hoping to avoid similar accidents happening again in the future.

Results and Discussion

Visual Inspection of the Failed Pipe

The appearance of the failed heating pipe is displayed in Fig. 3, whose design sizes were φ 20.0 mm $\times$ 2.0 mm. The inner and outer surfaces of the pipes away from the fracture were smooth, flat and clean, free from dents, bubbles, obvious scratches and other surface defects that affect performance, and there were no visible impurities. Table 1 shows the test results of the pipe wall thickness. Obviously, the wall thickness of more than half of the detection sites is thinner than the allowable range [21].

The failed pipe (Fig. 3a) exhibits certain degree of curvature, which is consistent with the structure of the coil, but the changing of the fracture section sizes, indicating that excessively bent has occurred. The cross section of the pipe was approximately transformed from a perfect circle to an ellipse-like shape with a long axis of 20.4 mm and a short axis of 19.3 mm. There is a clear crease on the opposite side of the fracture as shown in Fig. 3b; it can be speculated that the fracture at this position experienced rapid instability during the fracture process.

3-Dimensional Stereoscopic Inspection of the Failed Pipe

Cutting the failed PE pipe along the fracture section, the visual inspection of the fracture section was conducted by three-dimensional stereoscopic microscope. From Fig. 4a, it can be seen that there is a long stripe, which originating from the outer wall and finally ending at the inner wall, on one side of the fracture section, which side was named as I side. Strangely, there is no corresponding stripe being found on the opposite side of the fracture section as shown in Fig. 4b, and which side was named as II side.

Microstructure of the Failed Pipe

Scanning electron microscope (SEM) was used to further reveal the fracture mechanism of the failed pipe. Figure 5 shows the microscopic morphologies of the I side fracture section. Unlike the relatively flat and smooth inner wall,

Fig. 2 Appearance of floor heating pipe

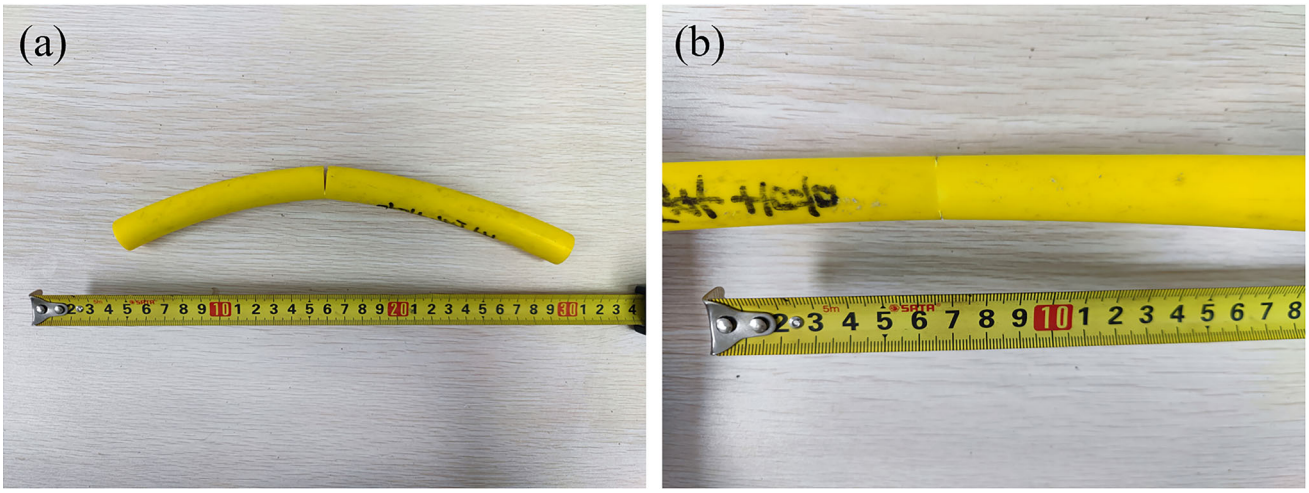

Fig. 3 (**a**) Side, and (**b**) opposite side of fracture appearance of failed pipe

Table 1 Wall thickness deviation of the failed pipe

Detection site	standard	1#	2#	3#	4#	5#	6#	7#	8#
Wall thickness deviation (mm)	0–0.3	− 0.1	0	− 0.1	0	0	− 0.1	− 0.1	− 0.1

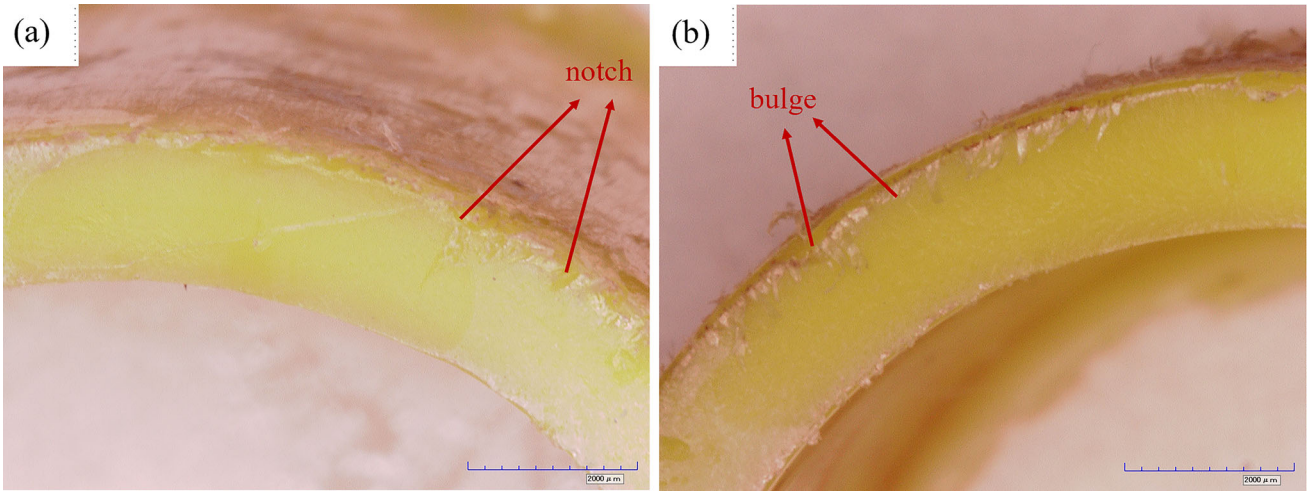

Fig. 4 Visual appearance of the fracture section under 3-dimensional stereoscopic microscope of (**a**) I side, and (**b**) II side

the outer wall of the failed pipe has a certain degree of defects. There is a notch as shown as shown in Fig. 5a on the outer wall of the pipe, and two stripes extend from this notch to the inner wall. The long stripe leads to the inner wall with a 30° angle, which is consistent with that shown in Fig. 4a, and the short stripe leads vertically to the inner wall and interrupted in the middle, which is not so clear as former under the three-dimensional stereoscopic microscope. Magnifying the notch (Fig. 5b and c), it can be observed that the short stripe is virtually composed of a series of inclusions. These inclusions are essentially fibrous tissues. Some holes of various sizes below the fibrous tissue indicate that the inclusions are not well combined with the polymer matrix, and delamination should occur during the fracture process. Once external stress is applied, those regions would become the source of stress concentration. In addition, many fine particles are also irregularly distributed on the matrix.

In order to determine the chemical compositions of the inclusions and the fine particles, EDS was performed in the location A, B and C, and the results are shown in Table 2. The chemical compositions of the fibrous tissues and fine particles are basically same, while the proportion of each element is quite different. Location A and B which represents the fibrous inclusions was detected with larger content of carbon, while location C which represents the fine particles was detected with larger content of nitrogen and oxygen. Weather in shape or in chemical compositions, fibrous inclusions and fine particles are two different types of inclusions with different causes, although they are both organic components.

Figure 5d shows the dimple morphology around the cut-off region of the short stripe, which is the typical morphology of ductile fracture. On the contrary, the dissociated morphology could be observed on the outer wall part. That is, the fracture section close to the outer wall shows dissociated morphology, while that close to the inner wall shows dimple morphology.

Different with the short stripe which is composed of fibrous inclusions, the long stripe is actual a craze morphology. As the range bounded by the red dashed box shown in Fig. 5e, there is a series of intermittent small pits with a size of several microns as the bridging region that induces crazing. The arrangement of these intermittent small pits indicates the path through which the presence of outer wall defects leads to the formation of crazing during fracture process. Meanwhile, there is a bulge with a size of about 100–150 μm in the middle of the crazing in Fig. 5f, which is a delamination morphology.

Figure 6 shows the microscopic morphologies of the II side fracture section. In Fig. 6a, several bulges can be observed on the outer wall of the fracture section, which just consistent with the notch at the corresponding location on I side. However, neither the long stripe nor the short stripe could be observed on the II side. As discussed above, the short stripe is virtually composed of a series of fibrous inclusions, and the failure to find a corresponding arrangement of inclusions on the II side indicates that the pipe might crack precisely along the interface of the inclusions and the matrix. The weak bonding force between the inclusions and the matrix leads to poor compatibility between the two.

In addition, there are several stripes developing in the circumferential and radial directions in the middle part of the II side fracture section. Some of these stripes are stripe-shaped holes with different depths, which are framed by red solid lines in Fig. 6b, and the substrates on both sides of these stripes are not completely on the same level. Although irregular-shaped inclusions can be observed on the fracture surface around the stripes, there are no obvious

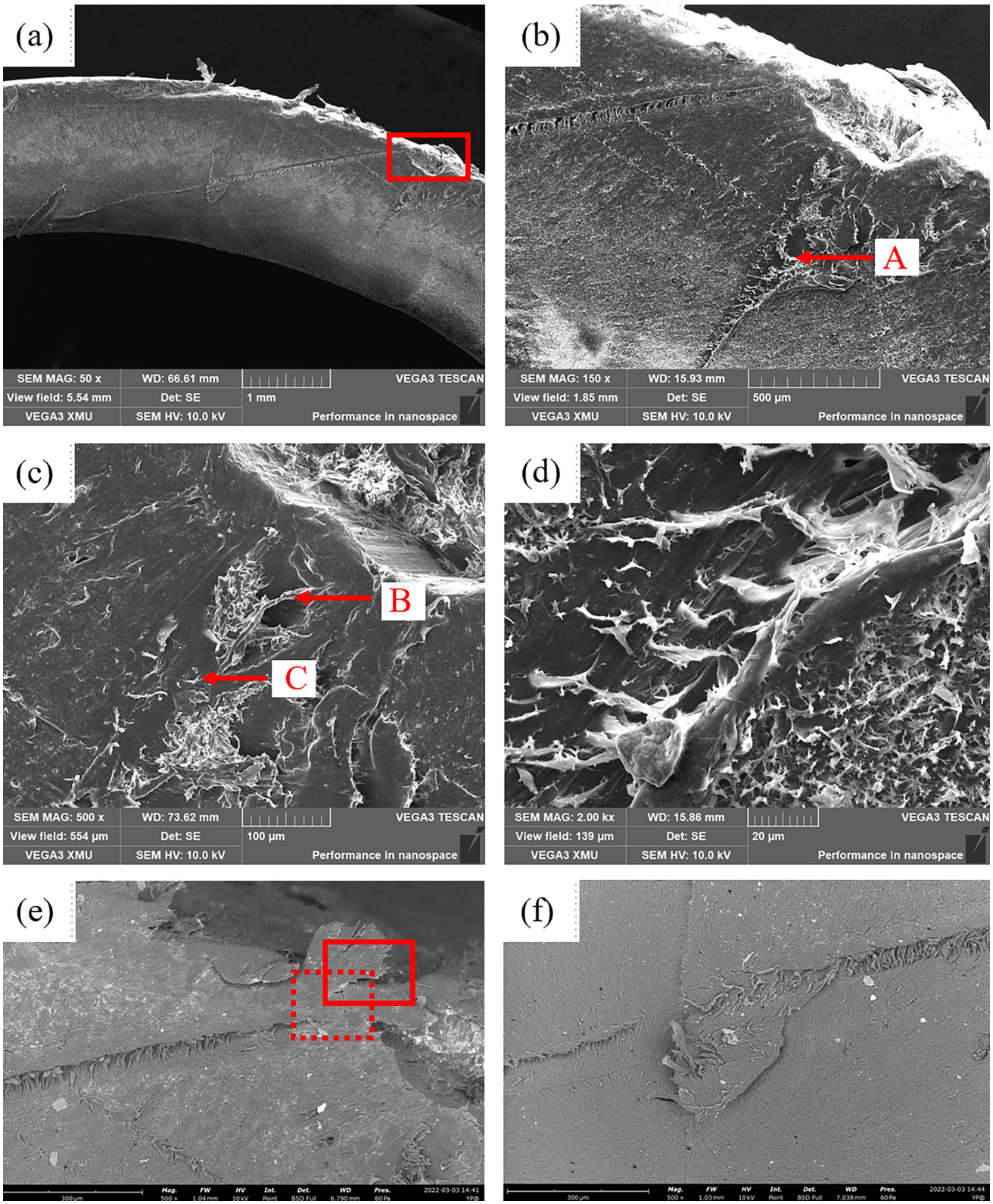

Fig. 5 Microscopic morphologies of I side of the failed pipe fracture section. (**a**) overall appearance (**b**) appearance of crack initiation source (**c**) fibrous aggregates and small-sized particles on the fracture surface (**d**) morphology of the short stripe in the cut-off region (**e**) craze propagation path from the crack initiation source and (**f**) bulge in the middle part of the long stripe

large-sized inclusions inside these strip-shaped cracks (Fig. 6c). Meanwhile, these inclusions are small in size and far away from each other (several times larger than their own scale); it is difficult to believe that the existence of these inclusions caused the generation of strip-shaped holes. According to relevant literature reports, due to the high shrinkage rate (0.02–0.05) of polyethylene, it is easy to introduce internal shrinkage holes during the molding process. Therefore, the appearance of these striped holes is most likely caused by shrinkage cavities during the molding process of polyethylene pipes.

Share D Hardness and Density of the Failed Pipe

The surface hardness of the failed pipe samples was measured by Shore D hardness tester, and the Shore D hardness of the failed pipe was about 60 (Table 3). The relatively low surface hardness of the failed pipe make the outer wall more susceptible to generate notches, pits, scratches, etc. The density of the failed pipe is 0.9319 g/cm^3 which is slightly lower than the technical standard (0.935–0.941 g/cm^3).

Table 2 Chemical compositions by EDS of the inclusions on the fracture section on I side (wt. %)

Element	C	O	N	Na	Si	Cl	K
A	94.92	2.00	3.08	…	…	…	…
B	84.19	9.58	5.15	0.53	0.42	0.13	…
C	68.69	18.98	9.66	0.86	…	0.22	1.58

Hydrostatic Test of the Failed Pipe

The purpose of the hydrostatic strength test is to measure the internal pressure resistance of the pipe, and to check whether the pipe meets the requirements of the service pressure level. The test was carried out under the conditions with temperature of 95°C and hoop stress of 3.55 MPa. After 3 min and 15 s, the sample ruptured, far from the requirement of maintaining no rupture and leakage for 165 h [21].

FTIR of the Failed Pipe

FTIR was conducted the chemical structural of the failed PE pipe for floor heating system. Figure 7 shows the FTIR spectra, which proved the material of the failed pipe is polyethylene. The main peaks present at 2912 cm^{-1} and 2849 cm^{-1}, which are, respectively, attributed to the CH_2 antisymmetric stretching vibration and CH_2 symmetric stretching vibration. CH_2 scissor vibration peak appears at 1472 cm^{-1}. The peak observed at 729 cm^{-1} and 717 cm^{-1} indicates the presence of the in-plane rocking vibration of CH_2, while the peak present at 729 cm^{-1} indicates the degree of the failed pipe's crystallinity is relatively weak.

Table 3 Shore D hardness of the failed pipe

	Test 1	Test 2	Test 3	Test 4	Test 5	Average value
Shore D hardness	57.5	60.5	61.5	61.0	60.5	60.2

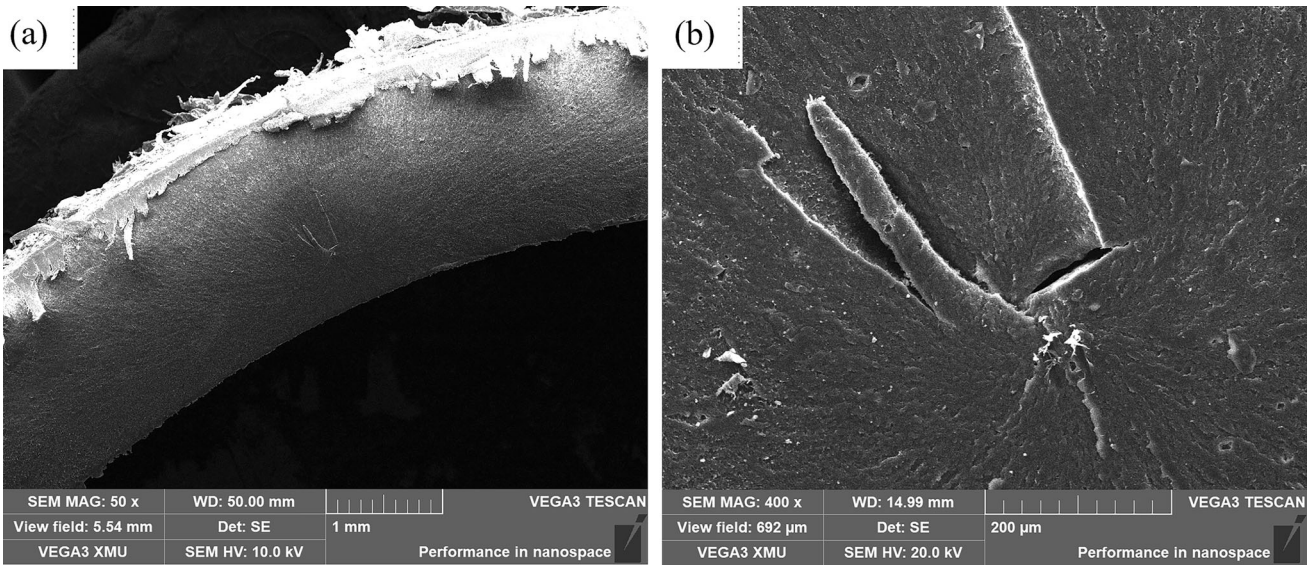

Fig. 6 Microscopic morphologies of II side of the failed pipe fracture section (**a**) overall appearance of the source of cracking, (**b**) crack concentration zone, and (**c**) Irregular inclusions near the crack concentration zone

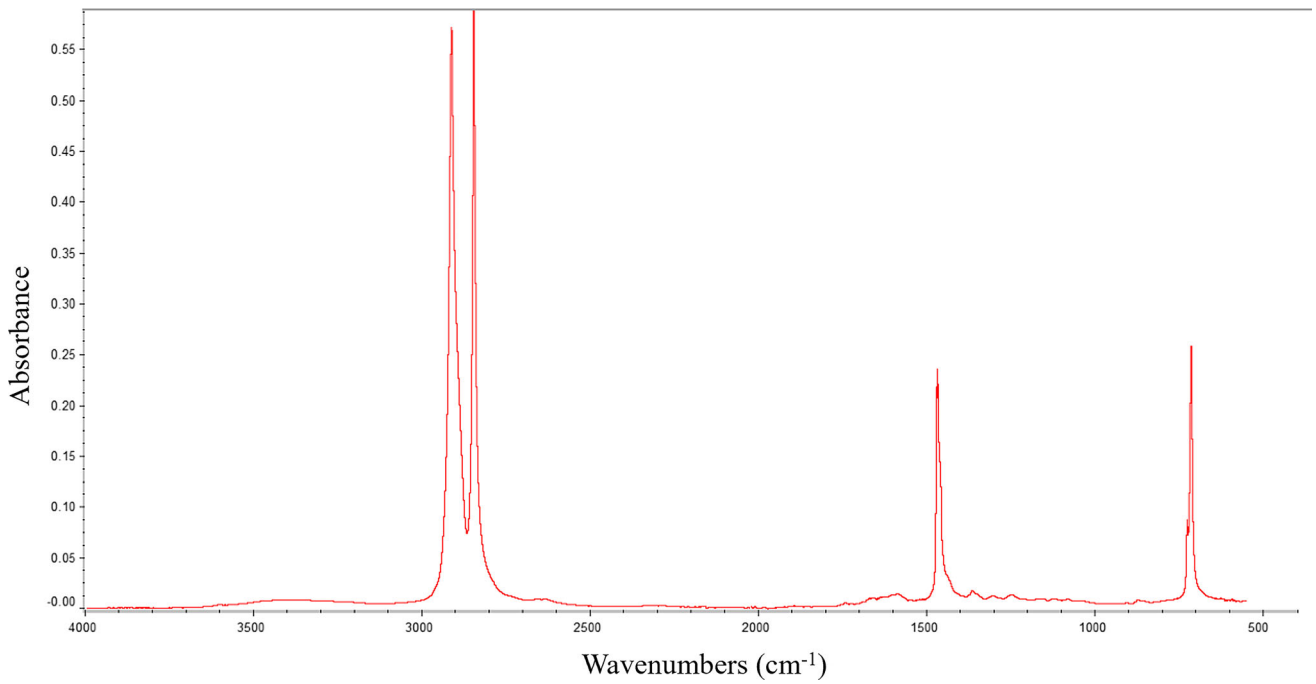

Fig. 7 FTIR spectra of the failed pipe

There is a series of weak CH_2 out-of-plane rocking vibration peaks between 1340–1150 cm^{-1}, which also indicates that the polymer pipeline is not completely crystallized, and the CH_2 groups are disordered and not completely arranged in a zigzag pattern [22]. Since in the FTIR results, we almost did not observe the existence of miscellaneous peaks, it can be seen that the purity of polyethylene in the failed pipe is very high.

TGA of the Failed Pipe

The failed pipe is analyzed by TGA. The temperature is specified from 40 °C to 500 °C under nitrogen environment, and the heating rate is 2 °C/min. As shown in Fig. 8, the initial decomposition temperature is about 200 °C and completely decomposed at 500 °C. When heated to 400 °C, the sample entered the accelerated decomposition stage and the temperature of the largest decomposition rate is about 480 °C. The result that there is nothing remaining after heating decomposition indicating that almost all the components of the failed pipeline are organic compounds, especially polyethylene, and almost no inorganic additives such as carbon black or carbides are contained.

DSC of the Failed Pipe

The mass crystallinity and the melting peak temperature of the failed pipe were obtained by DSC. The mass of the sample is 10.0 mg, and it was heated from ambient temperature to 175 °C with heating rate 2 °C/min. As shown in Fig. 9, the melting peak temperature of the failed pipe is 133 °C and the heat flow at which temperature is about 6 mW. The mass crystallinity of the failed pipe could be obtained by the following equation:

$$W_c = \frac{\Delta h}{\Delta h^0}$$

where Δh is the enthalpy of the fusion of the failed pipe and Δh^0 is the enthalpy of fusion of polyethylene with 100% crystallinity (293 J/g) [12]. Integrating the endothermic peak area shown in Fig. 9, the enthalpy of the fusion of the failed pipe can be obtained as 155 J/g. Correspondingly, the mass crystallinity of the failed pipe is 52.9%.

XRD of the Failed Pipe

Figure 10 shows the X-ray diffraction spectra of the failed pipe. Data was collected by detector system with a continuous scanning mode over a scattering angle (2θ) range from 10° to 80°, and copper was used as anode target material. When the value of 2θ angle equal to 21.45° and 23.84°, two main characteristic peaks appear on the XRD spectra, corresponding to the two crystal planes (110) and (200). Substituting the area of the crystalline peak and the amorphous peak into the following formulas, the crystallinity of the failed pipe can be calculated [23]:

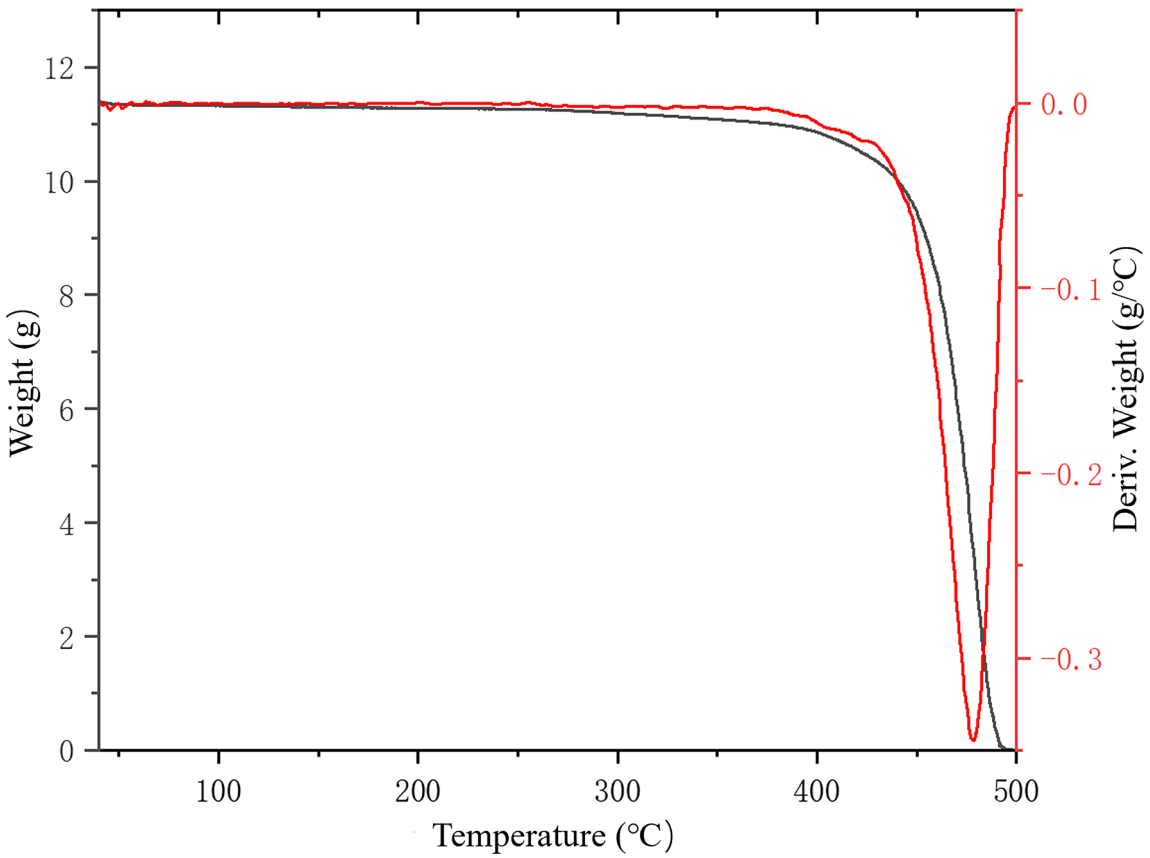

Fig. 8 The TGA analysis of the failed pipe

$$X_{cw} = \frac{I_c}{I_c + I_a}$$

$$I_c = K_1 S_{110} + K_2 S_{200}$$

$$I_a = K_3 S_a$$

where I_c is the intensity of crystal peak intensity, I_a is the intensity of amorphous peak, S_{110}, S_{200} and S_a represent the peak area of the crystal planes (110), (200) and amorphous peak, respectively. K_1, K_2 and K_3 are diffraction peak correction factors, which are correlation with 2θ angle at the same temperature. When the value of 2θ angle equal to 19.17°, the intensity of the amorphous peak is the highest. Substituting that value into the diffraction peak correction factor of the amorphous peak, the following ratio relationship can be obtained:

$$K_1 : K_2 : K_3 = 1 : 1.46 : 0.75$$

At last, the crystallinity of the failed pipe calculated by the XRD method is 53.9%.

NMR of the Failed Pipe

Since the spectral line corresponding to the crystalline region is wide in the NMR spectrum, while the spectral line corresponding to the amorphous region is narrow, the crystallinity of the polymer material can be determined based on the ratio of broad spectrum to narrow spectrum in the composite spectral line, which is usually calculated based on the relaxation time [24]. Table 4 shows the relaxation time and crystallinity of the failed pipe detected at − 70 °C, and the crystallinity calculated by the NMR method is 55.6%.

GPC of the Failed Pipe

GPC analysis was conducted to obtain the molecular weight distribution of the failed pipe. The mobile phase used in the test was heated trichlorobenzene (160 °C), and the solution concentration was 0.10 mg/ml with injection volume 100.0 μl. Figure 11 shows the weight average molecular weight distribution and Table 5 shows the value of number average molecular weight, weight average molecular weight and polydispersity coefficient. Obviously, its unimodal molecular weight distribution was inconsistent with the PE-RT requirements for bimodal molecular weight distribution [25]. Besides, its relatively low molecular weight made it prone to molecular chain movement resulting in poor mechanical properties.

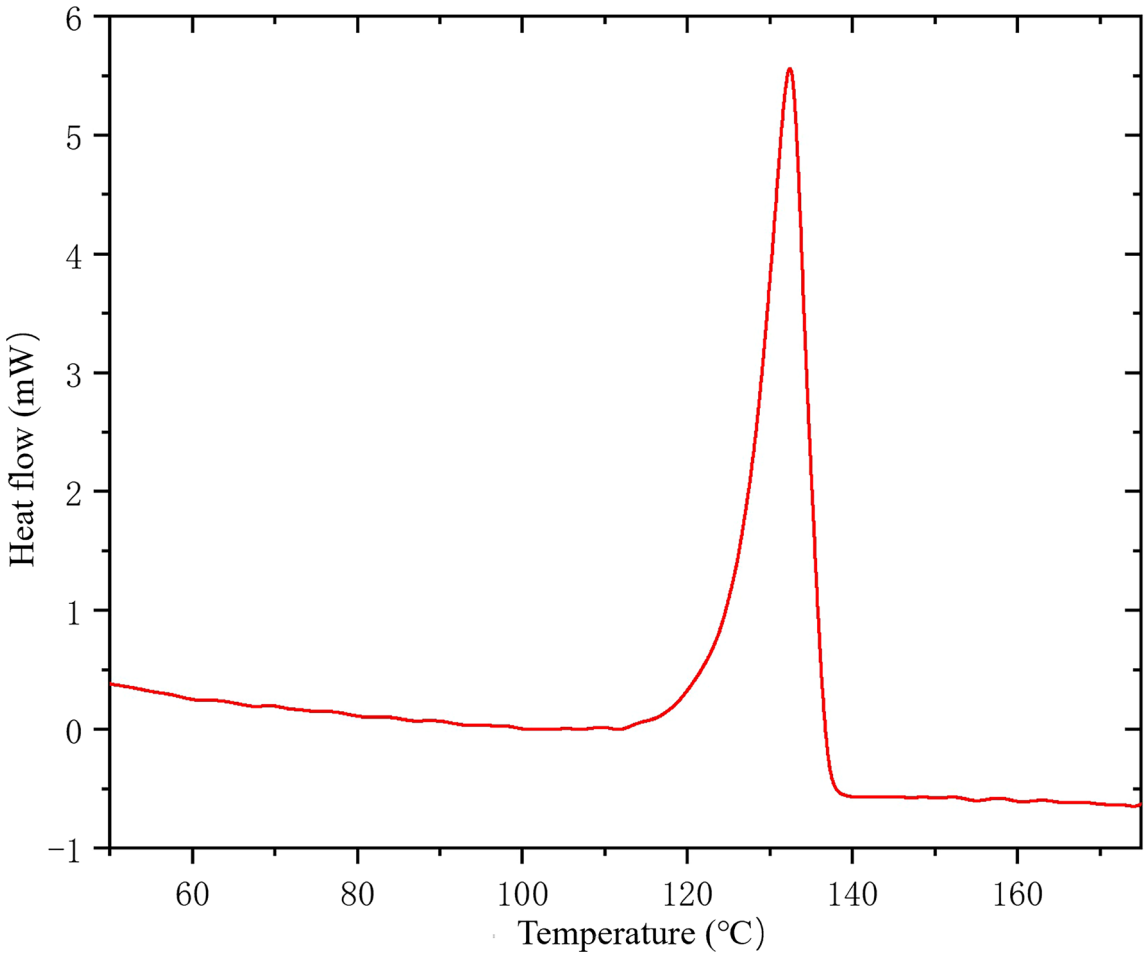

Fig. 9 The DSC analysis of the failed pipe

Failure Analysis

According to the results of FTIR, TGA and DSC, the material of the failed pipe for floor heating system is indeed polyethylene. However, the results of GPC show that this material does not meet the bimodal molecular weight distribution requirements of floor heating pipes at all. Based on the micromorphology analysis and mechanical properties analysis, the failure mechanism of the failed pipe should be slow crack cracking with defects.

Molecular Chain Disentangling and Brittle Fracture

Polyethylene has two main fracture modes: ductile fracture and brittle fracture [26]. Ductile fracture usually occurs when a large tensile stress is applied in a short period of time, while brittle fracture commonly occurs under a low tensile stress with a long period of time. Since the internal structure of macromolecules is variable under the action of external forces, the mode of polyethylene pipe fracture is time-dependent. The question is to compare the characteristic time for chain disentangling with the time it takes for the molecular chain to break under the external force. If the stress applied to the polymer material is large enough, before the polymer segments have adjusted their configuration and entangled with each other, the covalent bonds in the molecule have destroyed. On the contrary, if the force applied is not large enough to break the covalent bonds, the polymer chain will adjust its configuration under the traction of the tensile stress. At that time, the force that maintains the polymer material changes from chemical bonds to physical bonds and tensile strength decreases. If the applied tensile stress is enough to break the van der Waals bond that maintain the structure of the polymer material, then brittle fracture will occur. If the tensile stress is too small to break the van der Waals bond, the polymer material will not break. Meanwhile, when the applied tensile stress is relatively small, the time scale for the disentangling of the polymer chain will be correspondingly long (Table 6) [27, 28].

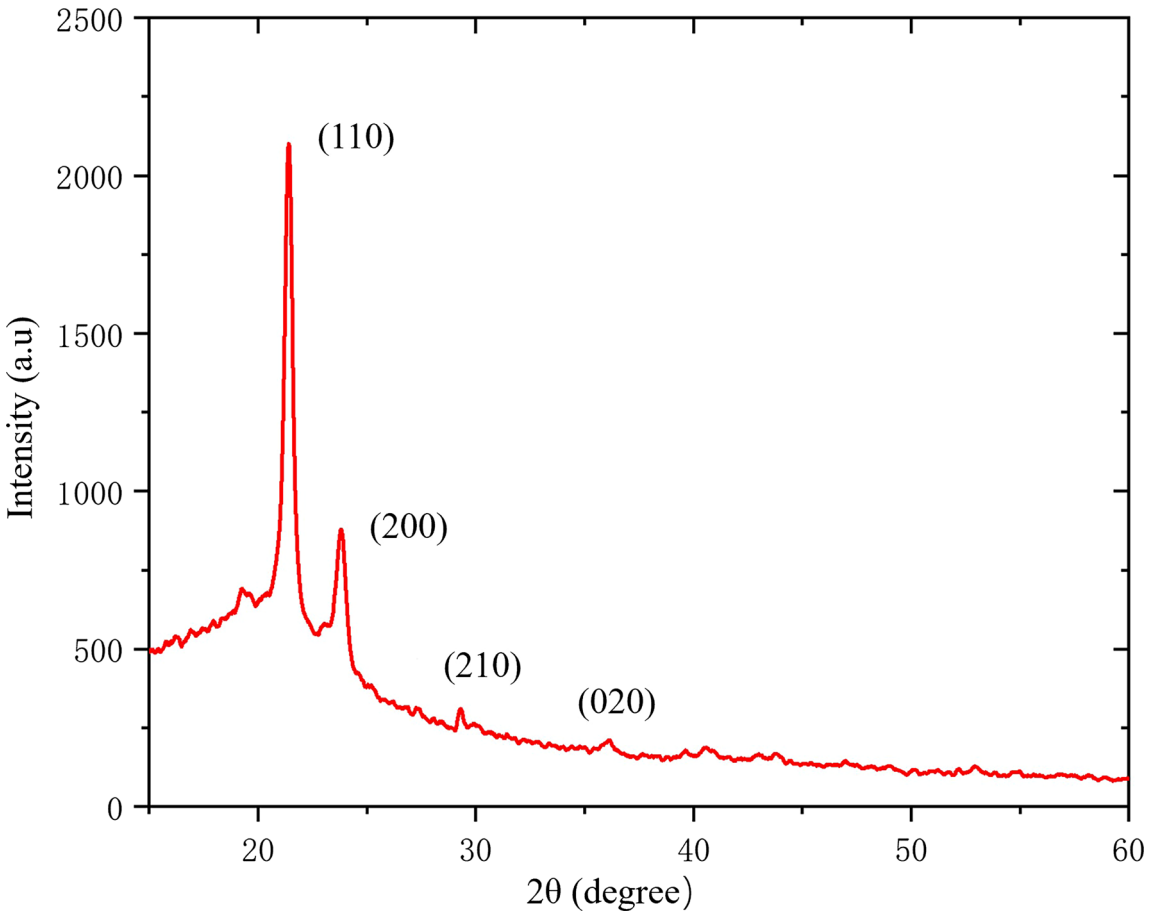

Fig. 10 XRD spectra of the failed pipe

Table 4 Crystallinity of the failed pipe

	Test 1	Test 2	Test 3	Average value
Relaxation time T_{21}	0.0095	0.0095	0.0094	…
Relaxation time T_{22}	0.0323	0.0325	0.0322	…
Crystallinity	55.64	55.80	55.44	55.63

As shown in Fig. 5b, the outer and inner fracture sections show the morphologies of brittle fracture and ductile fracture, respectively. Obviously, according to the above analysis, the tensile stress strength of the two is different. Since the failed pipe was excessively bent at the fracture, and the pipe wall on the fracture side was subjected to tensile stress. It can be further deduced that, in the early stage of fracture, the outer wall part suffered the action of small tensile stress in a relatively long time and occurred brittle fracture, and in the second half of the fracture process, the tensile stress on the fracture increases and ductile fracture would occur in a short period of time. The question is why the tensile stress on the inside and outside of the pipe wall is different.

Slow Crack Cracking with Defects

As shown in the following formula, the stress field around the crack tip can be described by linear elastic fracture mechanics (LEFM) [26, 29].

$$K_I = \sigma\sqrt{\pi a}Y(a/s)$$

where K_I is the stress intensity factor which describes the stress distribution around the crack tips, and the subscript I indicates that the sample is subjected to tensile stress, a is a crack length and $Y(a/s)$ is geometric factor which can be estimated numerically or found in literature. The crack growth curve can be described by Fig. 12; the horizontal and vertical coordinates are the logarithm of K_I and $\mathrm{d}a/\mathrm{d}t$, respectively. The crack growth behavior can be divided into three stages. In stage I which called threshold stage, the crack growth rate will fall rapidly to the value corresponding to the threshold value K_{Ith}. In stage II which called stable crack growth stage, the crack propagation rate can be described by the following formula:

$$\frac{\mathrm{d}a}{\mathrm{dt}} = A_1 K_I^m$$

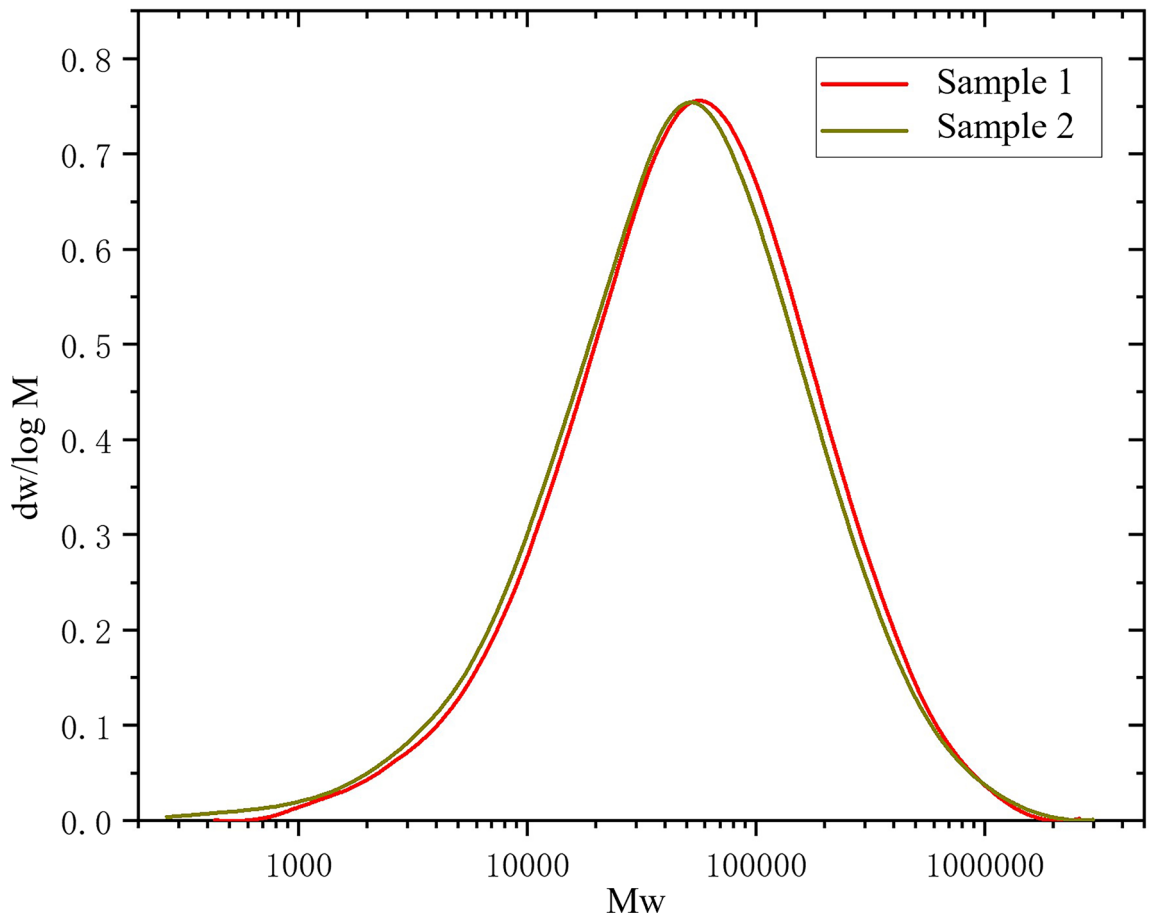

Fig. 11 GPC analysis of the failed pipe

Table 5 Molecular weight of the failed pipe

	Mn	Mw	PD
Sample 1	21,681	104,799	4.83
Sample 2	16,926	100,784	5.95

where A_1 and m are material constants, and A_1 is a function of temperature. When the influence of temperature is included, the above formula can be rewritten as:

$$\frac{\mathrm{d}a}{\mathrm{d}t} = A_2 K_I^m \exp\left(-\frac{Q}{RT}\right)$$

where A_2 is material constant, Q is termed the activation energy for crack growth and R is the gas constant, $8.31 J/\mathrm{mol}\cdot\mathrm{K}$. As temperature increases, the steady crack propagation rate increases[30]. The crack growth rate will rise sharping in stage III, since the K_I approaches to the critical value K_{IC}[31].

Based on the above analysis, the fibrous inclusions appearing in the pipe wall are the source of fracture defects. Since the fibrous inclusions are more concentrated in the part of outer wall, which means that the outer wall part would be subjected to larger tensile stress than the inner wall part. Therefore, it is easier for the outer wall part to obtain sufficient tensile stress for molecular chain disentangling and brittle fracture to occur (Table 6). As the crack grew and propagated, the strength of the tensile stress exerted on the fracture section would be amplified, so ductile fracture occurred at that moment. The crease on the opposite side of the fracture can prove that the failed pipe has undergone rapid buckling fracture. In addition, the EDS analysis of the inclusions showed that the fibrous inclusions contain large amount of oxygen and nitrogen (Table 1), so that they are polar. While polyethylene is non-polar. The polarity of the inclusions and the non-polarity of the matrix resulted in the interface incompatibility [32]. For this reason, the bonding force between the inclusions and the matrix would be weaker than that of the matrix itself, and weaker than that of the inclusions itself. Of course, during use, the hot water inside the pipe would increase the temperature of the pipe wall, thereby accelerating its crack propagation rate. Microscopically, that process occurs since high temperature promotes the

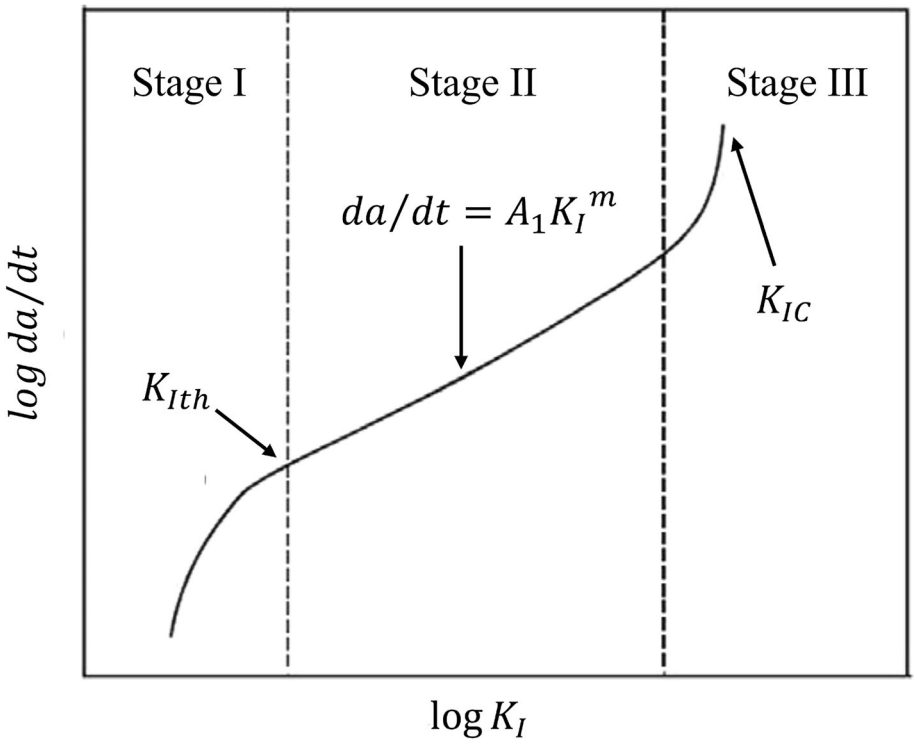

Fig. 12 Scheme of crack growth rate curve

Table 6 Effect of tensile stress strength on fracture behavior of polymer materials

Strength of tensile stress	Large	Medium	Small
Able to break covalent bonds or not?	Yes	No	No
Able to break van der Waals bonds or not?	Yes	Yes	No
Comparison of characteristic time between covalent bond breaking and polymer molecular chain disentangling	The former is shorter	The latter is shorter	…
Time elapsed before fracture occur	Short	Long	…
Fracture mode	Ductile fracture	Brittle fracture	No fracture

movement of molecular segments and thus accelerates the disentangling process of molecular chains.

Entanglement Density, Molecular Weight and Tensile Strength

The following formula can be used to describe the energy needed to create new surface in complete polymer material, that is the energy required to form cracks in the polymer material.

$$\Gamma = \gamma + \frac{1}{4}\upsilon_e U d$$

where Γ is the surface energy, γ represents the van der Waals cohesive energy between molecule chains, υ_e indicates the effective entanglement density of the material, which is positively related to the proportion of crystalline region, U is the energy required to break covalent bonds, and d is the average distance between effective entanglements [33]. Obviously, the surface energy will decrease with entanglement density decreasing.

The topology of the polymer entanglement can be discussed by Edwards tube model that every polymer segment is effectively confined by adjacent molecular segments to a tube-like region [34]. The diameter of that called tube can be interpreted as the end-to-end distance of an entanglement segment:

$$a \sim bN_e^{1/2}$$

The above formula is a scaling calculation. Where b is the Kuhn length which means that the length of a part when the chain is assumed to be freely connected, and that part is called Kuhn monomer. The Kuhn length of polyethylene is typically about 1.4 nm. N_e is the number of Kuhn monomers in an entanglement segment. Practically, the number of Kuhn monomers N_e in the polymer segment is

determined by the tube diameter a, which can also be regarded as the transverse fluctuation amplitude. Since the Edwards tube model consider the tube is composed of N/N_e sections with size a, the average contour length $\langle L\rangle$ is the product of the entanglement segment length a and the average number of entanglement segments per molecule N/N_e as the following formula:

$$\langle L\rangle \sim a\frac{N}{N_e} \sim \frac{bN}{\sqrt{N_e}}$$

The motion of the chain is confined in the tube along the contour of the primitive path, and the curvilinear diffusion coefficient D_c describes the motion of the chain.

$$D_c = \frac{kT}{N\zeta}$$

where $N\zeta$ is the Rouse friction coefficient characterizes the curvilinear motion of a polymer confined by surrounding chains. Reptation time τ_{rep} can be used to describe the time required for a chain to diffuse out of the original tube:

$$\tau_{rep} \sim \frac{\langle L\rangle^2}{D_c} \sim \frac{\zeta b^2 N^3}{kTN_e} = \frac{\zeta b^2}{kT}N_e^2\left(\frac{N}{N_e}\right)^3$$

The first part of the above equation $\frac{\zeta b^2}{kT}N_e^2$ named the Rouse time τ_e which indicates the time required for a segment to diffuse a distance equal to its own size. The following formula shows the ratio of the Reptation time τ_{rep} and the Rouse time τ_e, which value is the cube of the number of entanglements along the chain.

$$\frac{\tau_{\mathrm{rep}}}{\tau_e} \sim \left(\frac{N}{N_e}\right)^3$$

There is no doubt that the value of N/N_e is proportional to the molecular weight of the polymer chain, and $\tau_{\mathrm{rep}}/\tau_e$ is proportional to the cube of the molecular weight of the polymer chain. Therefore, for polymer with larger molecular weight, even if disentanglement occurs under the action of tensile stress, there are still enough effective entanglement sites on each chain to maintain the necessary mechanical strength of the material, while for polymer with lower molecular weight, fracture occurs at that time [35].

Shrinkage Phenomenon in Polymer Molding Process

In Fig. 6, shrinkage cavities can be observed inside the failed pipe. In the injection molding process, shrinkage cavity is a very common problem, mainly due to the following reasons: Firstly, if the design of the main runner, runner and gate of the mold is unreasonable, there will be shrinkage cavities caused by the injection pressure not fully acting on the molten material in the mold cavity [36]. Secondly, due to the poor thermal conductivity of polyethylene, uneven temperature distribution is also an important reason for shrinkage of products. When the wall thickness of the polyethylene pipe fittings is uneven, the thick wall part will cool more slowly than the thin wall part during the cooling process, so that the thick wall part is prone to shrinkage [37]. The failed pipe discussed in this paper has poor uniformity of wall thickness, which is likely to cause shrinkage cavities. Thirdly, when there is a local temperature difference in the mold, shrinkage cavities will also occur in the part where the mold temperature is high [36].

Particularly, for polymers with crystalline state such as polyethylene, crystalline structure is also an important factor affecting the shrinkage porosity of the product. Since the density of the crystalline area is larger than that of the amorphous area, the uneven density distribution will lead to shrinkage phenomenon inside the product. The nucleation radius of polymer crystallization grains is the main factor affecting polymer shrinkage, while the nucleation number of polymer crystallization is relatively less important [38]. The larger the nucleation radius after the crystallization of the polymer, the greater the crystallinity and the greater the shrinkage. Since the crystallization nuclei formed by polymer crystallization have a larger radial growth rate at higher temperatures, the polymer cooling rate should be as large as possible during the molding process, which can effectively prevent the polymer from being in the stage of high nucleation growth rate for a long time, so that the degree of shrinkage can be avoided as much as possible. The size of the crystal nucleus of the crystalline polymer can also be reduced by means of filling, blending, reinforcement modification, etc., thereby reducing the molding shrinkage.

Conclusions and Countermeasures

Conclusions

1. The root causes of the premature fracture are the molecular weight of the pipe materials is too low and does not own bimodal distribution. Hence, the mechanical properties of the failed pipe are not able to meet the working conditions.
2. The direct reason is excessive bending. In order to meet the wiring requirements, some pipe sections changed curvature from the initial state, causing that convex sides of these sections are always subjected to tensile stress during use.
3. Because of the existence of the polar fibrous inclusions at the fracture, the stress is locally amplified. Since the bonding force between the matrix and the inclusions is

weak, delamination would be easier to occur under the tensile stress and crack occurs in turn.

4. Due to the internal shrinkage cavity introduced in the molding process, the matrix is not ideally bonded, and then the tensile strength and other mechanical properties are lower than the integrity, which is another important reason.

Countermeasures

1. The material of the floor heating pipe must ensure that it has sufficient molecular weight and meets bimodal molecular weight distribution required for polyethylene of temperature resistance.
2. During installation and using, make sure that the pipe is not bent beyond the design allowable range.
3. In the production of floor heating pipes, the use of recycled materials should be avoided, especially those whose molecular weight is not up to the standard and containing fibrous inclusions.
4. During the molding process, appropriate molds and processing techniques should be selected to avoid leaving shrinkage cavity in the final product. For example, strengthen the injection pressure, keep the wall thickness of pipe fittings uniform and so on.

References

1. C. Flammer, Green bonds: effectiveness and implications for public policy. Environ. Energy Policy Econ. **1**(1), 95–128 (2020)
2. B. Wan, L. Tian, M. Fu et al., Green development growth momentum under carbon neutrality scenario. J. Clean Prod. **316**, 128327 (2021)
3. G. Halkos, S. Managi, C. Wilson, Growth and efficiency in resource economics. Resour. Conserv. Recycl. **134**, A4–A5 (2018)
4. International Energy Agency, Global Energy Review: CO_2 Emissions in 2021, https://www.iea.org/reports/global-energy-review-co2-emissions-in-2021-2. Accessed March, 2022
5. S. Shukla, R. Daneshazarian, A. Mwesigye et al., A novel radiant floor system: detailed characterization and comparison with traditional radiant systems. Int. J. Green Energy. **17**(2), 137–148 (2020)
6. T. Li, A. Merabtine, M. Lachi et al., Experimental study on the thermal comfort in the room equipped with a radiant floor heating system exposed to direct solar radiation. Energy. **230**, 120800 (2021)
7. M. Bojić, D. Cvetković, V. Marjanović et al., Performances of low temperature radiant heating systems. Energ. Build. **61**, 233–238 (2013)
8. P. Ding, Y. Li, E. Long et al., Study on heating capacity and heat loss of capillary radiant floor heating systems. Appl. Therm. Eng. **165**, 114618 (2020)
9. A. Vadiee, A. Dodoo, E. Jalilzadehazhari, Heat supply comparison in a single-family house with radiator and floor heating systems. Buildings. **10**(1), 5 (2019)
10. G. Zhou, J. He, Thermal performance of a radiant floor heating system with different heat storage materials and heating pipes. Appl. Energy. **138**, 648–660 (2015)
11. A.D. Ancas, F.E. Turcanu, M. Verdes et al., Comparative numerical studies on the structural behavior of buried pipes subjected to extreme environmental actions. Materials. **15**(9), 3385 (2022)
12. W. Yu, B. Azhdar, D. Andersson et al., Deterioration of polyethylene pipes exposed to water containing chlorine dioxide. Polym. Degrad. Stabil. **96**(5), 790–797 (2011)
13. Y. Wu, X. You, S. Zha, Mechanical behavior analysis of buried polyethylene pipe under land subsidence. Eng. Fail. Anal. **108**, 104351 (2020)
14. X. Liu, H. Zhang, M. Xia et al., Mechanical response of buried polyethylene pipelines under excavation load during pavement construction. Eng. Fail. Anal. **90**, 355–370 (2018)
15. H.H. Ya, A. Hafizzie, W. Pao et al., Experimental study on the impact of wet sand particle to the erosion of carbon steel and HDPE. AIP Conf. Proc. AIP Publish. LLC. **2030**(1), 020045 (2018)
16. L. Li, L. Qiao, J. Fan et al., Mechanical behavior of polyethylene pipes under strike-slip fault movements. Polymers. **14**(5), 987 (2022)
17. Z. Liang, Q. Yang, J. Zhang et al., Mechanical analysis of buried polyethylene pipelines under ground overload. J. Fail. Anal. Preven. **19**, 193–203 (2019)
18. X.L. Yang, S.H. Wang, Y. Gong et al., Effect of biological degradation by termites on the abnormal leakage of buried HDPE pipes. Eng. Fail. Anal. **124**, 105367 (2021)
19. Y. Gong, S.H. Wang, Z.Y. Zhang et al., Degradation of sunlight exposure on the high-density polyethylene (HDPE) pipes for transportation of natural gases. Polym. Degrad. Stabil. **194**, 109752 (2021)
20. Y.M. Mo, Y. Gong, Z.G. Yang, Failure analysis on the O-ring of radial thrust bearing room of main pump in a nuclear power plant. Eng. Fail. Anal. **115**, 104673 (2020)
21. BS ISO 22391–2:2007, Plastics piping systems for hot and cold water installations-polyethylene of raised temperature resistance (PE-RT). Part 2: Pipes
22. M. Eguiluz, H. Ishida, A. Hiltner, Infrared-analysis of brominated polyethylene single-crystals. J. Polym. Sci. Pol. Phys. **175**(5), 893–897 (1979)
23. E.J. Joseph, K. Panneerselvam, Effect of particulate fillers on mechanical, metallurgical and abrasive behavior of tungsten reinforced HDPE composites: a Taguchi approach. Mater. Today Proc. **39**, 1228–1234 (2021)
24. S. Golotvin, A. Williams, Improved baseline recognition and modeling of FT NMR spectra. J. Magn. Reson. **146**(1), 122–125 (2000)
25. B. Paredes, J. Moreno, A. Carrero et al., Evaluation of bimodal polyethylene from chromium oxide/metallocene hybrid catalysts for high resistance applications. Macromol. React. Eng. **14**, 2000032 (2020)
26. A. Frank, W. Freimann, G. Pinter et al., A fracture mechanics concept for the accelerated characterization of creep crack growth in PE-HD pipe grades. Eng. Fract. Mech. **76**(18), 2780–2787 (2009)
27. H. Zhang, Z. Zhou, A. Chudnovsky, Applying the crack-layer concept to modeling of slow crack growth in polyethylene. Int. J. Eng. Sci. **83**, 42–56 (2014)
28. A. Chudnovsky, Y. Shulkin, Application of the crack layer theory to modeling of slow crack growth in polyethylene. Int J Fracture. **97**(1), 83–102 (1999)
29. P. Hutař, M. Ševčík, L. Náhlík et al., A numerical methodology for lifetime estimation of HDPE pressure pipes. Eng. Fract. Mech. **78**(17), 3049–3058 (2011)

30. D. William, J.R. Callister, G. David et al., *Fundamentals of Materials Science and Engineering* (Wiley, New York, 2015), p.364–365
31. Z.P. Bažant, L.F. Estenssoro, Surface singularity and crack propagation. Int. J. Solids. Struct. **15**(5), 405–426 (1979)
32. Y. Koutsawa, S. Tiem, W. Yu et al., A micromechanics approach for effective elastic properties of nano-composites with energetic surfaces/interfaces. Compos. Struct. **159**, 278–287 (2017)
33. R.A.C. Deblieck, D.J.M. Van Beek, K. Remerie et al., Failure mechanisms in polyolefines: the role of crazing, shear yielding and the entanglement network. Polymer. **52**(14), 2979–2990 (2011)
34. D.W. Mead, D. Yavich, L.G. Leal, The reptation model with segmental stretch. Rheol. Acta. **34**, 360–383 (1995)
35. M. Rubinstein, R.H. Colby, *Polymer Physics* (Oxford University Press, Oxford, 2003), p.361–363
36. K.M. Jansen, D.J. Dijk, M.H. Husselan, Effect of processing conditions on shrinkage in injection molding. Polym. Eng. Sci. **38**(5), 838–846 (1998)
37. A. Tumbull, A.S. Maxwell, S. Pilai, Residual stress in polymer-evaluation of measurement technuques. J. Mater. Sci. **34**(3), 451–459 (1999)
38. M.D. Azaman, S.M. Sapuan, S. Sulaiman et al., Shrinkages and warpage in the processability of wood-filled polypropylene composite thin-walled parts formed by injection molding. Mater. Design. **52**(24), 1018–1026 (2013)